Phase transition at 350 K in the $Ti_3C_2T_x$ MXene: Possible sliding or moiré ferroelectricity

Francesco Cordero,[1,*] Hanna Pazniak,[2] Thierry Ouisse,[2] Jesus Gonzalez-Julian,[3] Aldo Di Carlo,[1] Viktor Soprunyuk,[4] and Wilfried Schranz[4]

[1]*Istituto di Struttura della Materia-CNR (ISM-CNR), Area della Ricerca di Roma - Tor Vergata, Via del Fosso del Cavaliere 100, I-00133 Roma, Italy*

[2]*Université Grenoble Alpes, CNRS, Grenoble INP, LMGP, 3 parvis Luois Néel, F-38000 Grenoble, France*

[3]*Department of Ceramics, Institute of Mineral Engineering, RWTH Aachen University, D-52074 Aachen, Germany*

[4]*Faculty of Physics, University of Vienna, Boltzmanngasse 5, 1090 Wien, Austria*

(Received 23 October 2023; accepted 2 January 2024; published 18 January 2024)

A phase transition is found in $Ti_3C_2T_x$ MXene at 350 K, by measuring the complex Young's modulus of self-standing thick films. A steplike softening and increase of the mechanical losses is found below 350 K, indicative of a phase transition, where the square of the order parameter is coupled to strain. It is argued that it should be a ferroelectric transition, most likely of the sliding (moiré) type, due to charge transfer between facing flakes sliding with respect to each other. If the transition will be confirmed to be ferroelectric, $Ti_3C_2T_x$ will be added to the class of metallic ferroelectrics and open new perspectives of applications, in addition to the numerous already studied.

DOI: 10.1103/PhysRevB.109.024105

I. INTRODUCTION

Up to recent times it was believed that ferroelectric transitions cannot occur in materials with sizes below a certain limit. The critical thickness for a film to sustain ferroelectricity (FE) was believed to be of the order of tens of nanometers in ferroelectrics with perovskite or fluorite structure, though new experiments revealed ferroelectricity at progressively smaller thicknesses [1,2], even down to the monolayer for $BiFeO_3$ [3]. After the prediction of FE with giant piezoelectricity in the monolayer chalcogenides SnSe, SnS, GeSe, and GeS [4] and the experimental verifications that $CuInP_2S_6$ has a FE transition with $T_C = 320$ K [5,6], the number of layered van der Waals (vdW) ferroelectrics has increased and includes α-In_2Se_3 [7], γ-InSe [8], SnS [9], SnSe, SnTe [10], 1T′-$MoTe_2$ [11], 1T′-MoS_2 [12], and 1T′-WTe_2 [13,14]. It has also been ascertained that in BN [15], MoS_2 [16], WTe_2, and a few other systems a new mechanism, other than lattice instability, is responsible for FE, namely the relative sliding of the vdW stacked layers, called sliding or moiré FE [17–20] and can even be observed in multilayers of monoatomic graphene [21]. The phenomenon was first predicted for BN and mixed BN/graphene bilayers and other vdW bilayers [22] and is based on the charge transfer between the facing atoms in the two layers, which induces an out-of-plane polarization. The interest in these ferroelectric mono- and bilayers is great, in view of possible applications in nanoelectronics [19,23], for example, more miniaturized FeRAMs integrable with Si or other materials thanks to the vdW coupling. Especially the sliding or moiré FE offers unique advantages of robust out-of-plane polarization [18,24].

MXenes are other two-dimensional (2D) layered materials with chemical formula $M_{n+1}C_nT_x$ (M standing for a transition metal, X standing for C or N, and T_x is surface functional groups). In the MXene structure, the surface groups T_x (usually –F, = O, –OH), inherited from the etching environment, are covalently bound to the transition metal and weakly bound via van der Waals bonds to terminations of neighboring sheets. Such structures are being extensively studied for a multitude of possible applications in important sectors [25], such as electrodes in Li/Na batteries [26], intermediate layers of perovskite solar cells [27], flexible and nanoelectronics [28], soft robotics [29], catalysis, and many others [25,26]. However, no ferroelectricity has been found up to now in MXenes, but only theoretically predicted in Sc_2CO_2 [30]. On the other hand, $Ti_3C_2T_x$ monolayers have been demonstrated to be piezoelectric [31,32]. Piezoelectricity, namely an induced strain proportional to an applied electric field or polarization induced by stress, is a consequence of FE, but is also possible in nonferroelectrics lacking spontaneous polarization, if their lattice belongs to certain noncentrosymmetric classes. This is the case of biatomic hexagonal layers and of $Ti_3C_2T_x$ [31].

It must be said that the theoretical predictions of 2D FE are more numerous than the experimental verifications, which are rather challenging. In fact, these types of FE are probed on mono-, bi- or trilayer nanoflakes with techniques such as piezo-force microscopy (PFM) or conductive atomic-force microscopy (AFM).

We will show that these types of FE can be probed also with the simple macroscopic method of measuring the elastic anomaly associated with the FE transition on thick films of the layered material. We present the first measurements of the complex Young's modulus versus temperature of self-standing thick films of the $Ti_3C_2T_x$ MXene, which exhibit a clear and robust nearly second-order phase transition at

*francesco.cordero@ism.cnr.it

 ©2024 American Physical Society

$\simeq$ 350 K, and it is argued that, in spite of the good electrical conductivity, the transition should be ferroelectric, likely of the sliding type.

II. EXPERIMENTAL

A. Preparation of the MXene phase

$Ti_3C_2T_x$ MXenes were synthesized by selective chemical etching of the Al layer from a parent Ti_3AlC_2 powder precursor using the minimally intensive layer delamination approach [33]. To produce a thick $Ti_3C_2T_x$ film, a suspension of well-delaminated flakes was vacuum filtered through a nitrocellulose membrane with an average pore size of 0.22 μm. After drying, deposited layers were detached from the membrane, and a rigid thick free-standing MXene film was obtained. The film thickness was controlled by the concentration and the amount of filtered suspension.

B. Anelastic measurements—free flexural resonance

The complex Young's modulus $E = E' + iE''$ was measured in an apparatus where a bar-shaped sample is suspended on thin thermocouple wires in high vacuum ($<10^{-5}$ mbar), and electrostatically excited on its free-flexural resonant modes [34]. The resonance frequencies are $f \propto \sqrt{E}$ [35], so that the temperature dependence of E is evaluated as $E(T)/E_0 = [f(T)/f_0]^2$. The elastic energy loss coefficient $Q^{-1} = E''/E'$ is measured from the decay of the free oscillations or the width of the resonance peak. The measurements are made well within the linear elastic limit. Details on some of the experimental difficulties encountered and their solutions can be found in the Supplemental Material [36]. The measurements reported here were made on a strip 25.5 mm long, 3 mm wide, and (73 ± 4) μm thick, with the first three free-flexural resonances clearly visible. In order to consolidate the film avoiding warping and bubbles [36], the sample was put between two alumina slabs and heated at 1.5 °C/min up to 700 °C in 10^{-6} mbar, kept 1 h and furnace cooled. The film became flat and more brittle. Thermal annealing has been reported to improve electrical conductivity of MXene films and we observed the same trend in the change in Young's modulus: after annealing it increased from 11.9 GPa to 44 GPa, presumably due to the loss of intercalated species.

C. Dynamic mechanical analyzer

The anelastic spectra were measured also using a Perkin-Elmer Diamond Dynamic Mechanical Analyzer (DMA) in the three-point bending mode, where flexural vibrations are forced at fixed frequencies in the range 0.1–10 Hz in Ar atmosphere [36]. The samples were also characterized before and after the anelastic measurements by XRD, and Raman spectroscopy [36].

III. RESULTS

A. Free-flexural resonance

Figure 1 presents the Young's modulus E and elastic energy loss Q^{-1} measured during the first and third cooling runs (empty symbols), and subsequent heating (filled symbols). In

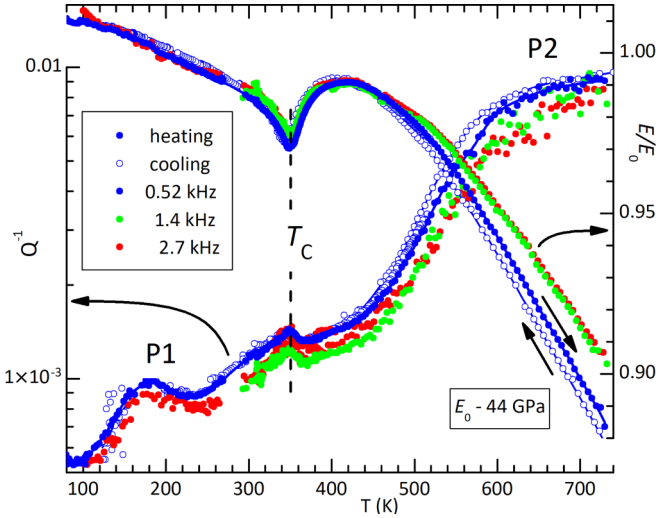

FIG. 1. Normalized Young's modulus and elastic energy loss measured during the fourth heating (filled symbols), exciting the first, second, and third flexural modes. The empty symbols are the first and third coolings.

the last case, in addition to the fundamental also, the second and third flexural modes were excited at higher frequencies. Until the sample was maintained in vacuum, the measurements were well repeatable, with some hysteresis between heating and cooling above room temperature. The main result is the nearly frequency-independent negative step of E and positive step of Q^{-1} below $T_C \simeq 350$ K. The step in E is preceded by a precursor softening extending tens of kelvin above T_C. This is the typical signature of a phase transition whose squared order parameter is linearly coupled with strain [37,38].

Above T_C the Young's modulus exhibits some frequency dispersion, that may be at least partly accounted for by the intense relaxation process labeled P2. In fact, this broad peak shifts to higher temperature with increase of frequency, indicating thermal activation of the spectrum of characteristic times and must be accompanied by a decrease of the real part, according to the Debye formula $\Delta E \propto (1 + i\omega\tau)^{-1}$ in the case of a single relaxation time τ ($\omega = 2\pi f$). There is also a minor peak in Q^{-1}, labeled P1, too small to produce visible effects on E. Also, P1 seems thermally activated, with a broad spectrum of relaxation times; it might be due to extended defects within the MXene layers, but the available data are insufficient to draw any conclusion.

These measurements have been repeated several times, to check their reproducibility also after exposure to air or immersion in water [36]. In brief, it was found that the anelastic spectrum was reproduced even when measured in 700 mbar water vapor up to 430 K, with little or no intercalation of H_2O. One-day immersion in water resulted in intercalation of ~0.3 H_2O per formula unit, softening the modulus and strongly depressing the elastic anomaly at T_C. Outdiffusion of water in vacuum was fast above 430 K. The cycle of experiments was concluded with heating up to 890 K, after which the original Q^{-1} curve was completely recovered, but E remained ~4% softer and the step amplitude was smaller than

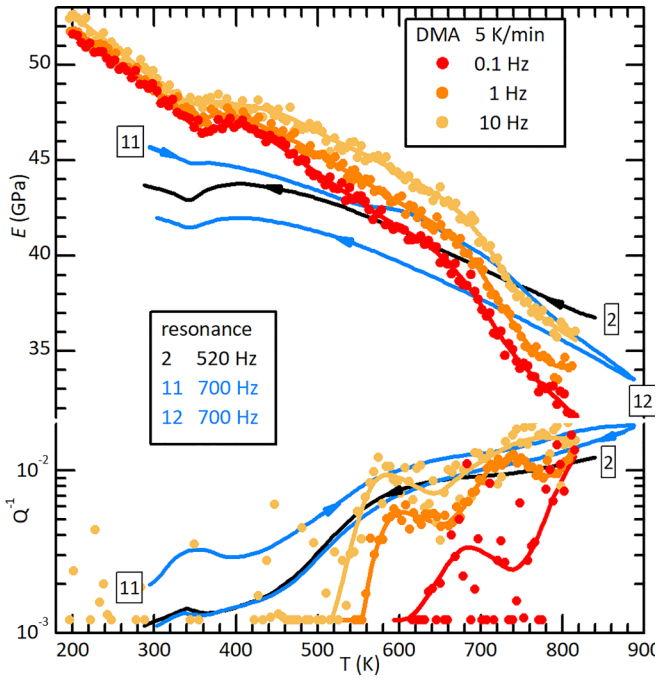

FIG. 2. Young's modulus and elastic energy loss measured with DMA at three frequencies heating at 5 K/min. The previous first and last runs with the resonance method are also shown, numbering the temperature scans in the same manner as in Fig. S1 [36].

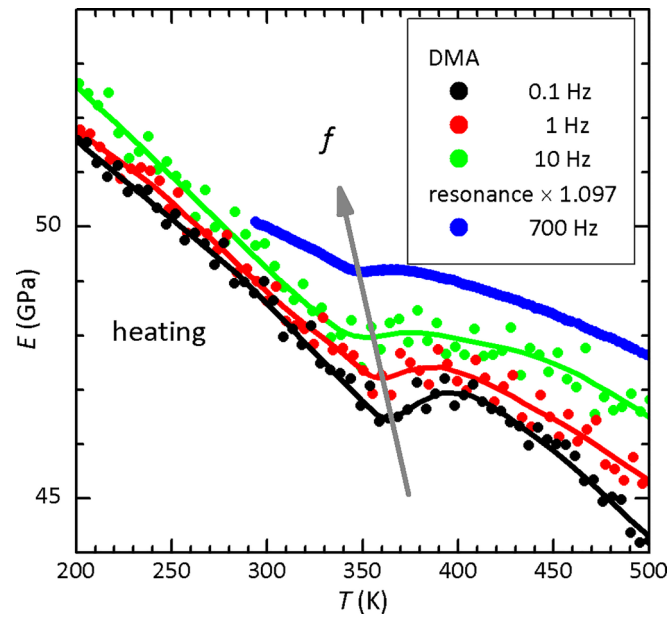

FIG. 3. Frequency dependence of the step in the Young's modulus at the phase transition. The resonance data are multiplied by 1.097.

originally (curve 12 in Figs. 2 and S1 [36]). This was probably also due to surface oxidation of the film, revealed by Raman spectroscopy after completing the anelastic measurements.

B. DMA

The DMA measurements substantially confirm all the previous ones with the resonance method, and provide additional information on the relatively slow dynamics characterizing the transition. A strip of as-prepared material had at room temperature a Young's modulus as low as 4 GPa, which increased up to 25 GPa after warming up to 495 K (not shown), confirming the consolidation effect of heating the as-deposited MXene sheet in vacuum or inert atmosphere. Figure 2 presents a DMA run from 200 to 810 K at 5 K/min and 0.1, 1, 10 Hz on the same sample that had been measured with the resonance method. Two months passed between the two sets of measurements. For comparison, the first and last runs with the resonance method are also shown, with the same labeling of Fig. S1 [36]. The major result is the confirmation of the steplike softening below 350 K. The magnitude of the modulus measured with the two methods is also in fair agreement, considering that the $E(T)$ curves are quite reproducible until the sample is measured and continuously kept in high vacuum, but otherwise they can vary considerably.

The DMA measurements put in evidence a progressive stiffening of E with increase of frequency above T_C and a broad step around 700 K, that had appeared also in the last resonance heating (curve 11).

More interesting is the frequency dispersion at the phase transition, put in evidence in Fig. 3. The last heating with the resonance method (curve 11 of Fig. 2) is multiplied by 1.097 for clarity. A 10% difference in the magnitude of the Young's moduli measured with the two methods may be due to imperfect shape and homogeneity of the sample and is well within the 20% estimated absolute accuracy of the DMA method [39]. In addition, it may be partly due to the variability of the modulus following exposure to air and high temperature cycles.

C. X-ray diffraction, Raman

X-ray diffraction (XRD) and Raman spectra were measured again after the above experiments [36]. The XRD spectra did not show any new peak, excluding decomposition and formation of new phases within the bulk of the film, but were shifted, indicating a decrease of the c lattice parameter from 26.35 to 20.22 Å . This is due to the loss of the initial intercalants. The Raman spectra, probing only the surface, exhibited new peaks attributable to TiO_2 (atanase), absent in the XRD spectrum, indicating that surface oxidation occurred.

IV. DISCUSSION

The major result of these anelastic measurements is the presence of a previously unnoticed nearly second-order phase transition at $T_C \simeq 350$ K.

The elastic anomaly consists of a negative step of ∼4% in the Young's modulus E below T_C, accompanied by a positive step in the elastic energy loss Q^{-1} and preceded by precursor softening extending tens of kelvin above T_C. This type of anomaly is characteristic of a phase transition whose order parameter (OP) P is coupled with strain ϵ through a term $\propto \epsilon P^2$ in the free energy [37]. This is the case of a ferroelectric transition where P is the electric polarization, but also of a (anti)ferromagnetic or antiferrodistortive transition (like octahedral tilting in perovskites [40]).

A magnetic transition can be excluded, since MXenes are mainly Pauli paramagnets. In some cases the magnetization of $Ti_3C_2T_x$ is very small down to 60 K, where a small kink may indicate a paramagnetic-to-antiferromagnetic transition [41].

Regarding the possibility of an antiferrodistortive transition in vdW solids, we know of only two possibilities in layered organic-inorganic halide perovskites. One is coordinated Jahn-Teller distortions of the BX_6 octahedra [42], but this is not possible with Ti^{4+}. The other is tilting of the octahedra [43]. This type of transition is common in perovskites AMX_3 [44], with short strong M-X bonds and longer weaker A-X bonds. When the network of rigid corner-sharing octahedra MX_6, sharing only their vertices X, cannot follow the thermal contraction of the more anharmonic A-X bonds, the rigid octahedra tilt in order to fit into the smaller lattice, giving rise to the antiferrodistortive transition. In $Ti_3C_2T_x$ there are only Ti-C bonds, and the network of edge sharing CTi_6 octahedra [45] has neither the structural flexibility nor a driving force for an antiferrodistortive instability. Indeed, deviations from the in-plane hexagonal structure have never been reported, neither with traditional x-ray diffraction nor with its pair distribution function analysis [46].

Therefore, the remaining possibility is that the transition is ferroelectric. Indeed, the elastic anomaly in $Ti_3C_2T_x$ is very similar to that found in classical ferroelectrics, for example in $BaTiO_{3-\delta}$, observable both in the insulating state with $\delta = 0$ [47] and when the material is made metallic by introducing O vacancies [48]. The similarity is not limited to the steps in elastic modulus and damping, but includes a precursor softening extending at least tens of kelvin above T_C [47,49]. The major difference between the elastic anomalies in $Ti_3C_2T_x$ and $BaTiO_{3-\delta}$ is the magnitude of the softening, which is up to 50% in $BaTiO_3$ and ~4% in $Ti_3C_2T_x$.

The ferroelectric nature of the transition, however, cannot be ascertained with the usual electric methods, since $Ti_3C_2T_x$ is a good electric conductor and any applied electric field is shielded by the free charge carriers. There are only few known metallic ferroelectrics, among which is the vdW layered WTe_2 [14]. Probing FE in vdW layered materials is achieved through sophisticated experiments on mono-, bi- and trilayer nanoflakes, but the task is particularly challenging in the case of electrically conducting materials. The present results show that the possible ferroelectric transition in $Ti_3C_2T_x$ can be probed also with a macroscopic measurement like the temperature dependence of the complex elastic modulus of a self-standing thick film. Not only it is not necessary to probe the polarization switching at the atomic level, but the good electric conductivity of the sample, which hinders the transition to the usual electrical methods, does not affect the elastic properties, which therefore reveal the elastic anomaly from the coupling between strain and polarization.

As far as the elastic anomaly is concerned, FE in $Ti_3C_2T_x$ may be due to the usual lowering of the symmetry of the paraelectric phase, like Ti off-centering in $BaTiO_3$ or vertical shifting of the intermediate Se plane in the vdW In_2Se_3 [50]. In the present case, a possibility would be vertical shifting of the C planes with respect to the Ti planes. This type of polar structure, however, has never been reported for $Ti_3C_2T_x$; rather, it has been found that monolayers are piezoelectric with null polarization in the absence of strain [31]. This corresponds to intrinsic piezoelectricity rather than switchable spontaneous polarization within a monolayer.

$Ti_3C_2T_x$ presents similarities with bilayer WTe_2, which is both semimetallic and ferroelectric with $T_C \simeq 350$ K [13,17]. The origin of its FE has been identified with the relative sliding between layers, which forms out-of-plane electric dipoles, due to the transfer of electronic charge between the facing atoms. The fact that the electric dipoles are formed between pairs of layers and approximately perpendicular to them explains why the polarization is not completely screened by the in-plane conductivity [17]. Relative sliding of two facing monolayers can switch the polarization over an extended area without requiring atomic displacements within the monolayers. A clear indication that the transition is due to an interlayer mechanism, and not intrinsic of each layer, is the fact that it is not observed in the as-prepared state, abundantly intercalated, and disappears by intercalating water.

The Curie temperature in sliding FE is well above room temperature, even though the sliding barrier is of $\lesssim$ meV [17]. This is very convenient for applications, since it combines low switching fields with robust ferroelectricity, and has been explained in the framework of continuum electromechanics as a consequence of the large in-plane rigidity of the layers [24]. For $Ti_3C_2T_x$ there would be the complication that the facing species are not the ordered planes of surface Ti atoms but the –OH, = O, and –F terminations. We are not aware of reports of sliding FE between nonuniformly terminated layers, but will discuss the elastic anomaly in this light, though the analysis will be valid for any type of FE. In fact, we can exploit the fact that in semiconducting bilayer WSe_2, exhibiting sliding FE, the spontaneous polarization $P(T)$ can be fitted with the usual Landau free energy with terms up to the sixth power of P [51],

$$F = \frac{a}{2}(T - T_C)P^2 + \frac{B}{4}P^4 + \frac{C}{6}P^6, \tag{1}$$

generally used for describing any first- ($B < 0$) or second-order ($B > 0$) ferroelectric transition. Once the transition is phenomenologically described in terms of Eq. (1), the elastic anomaly can be evaluated introducing a suitable coupling between stress/strain and order parameter P. We disregard a possible coupling of P with the "intrinsic" piezoelectricity found in the noncentrosymmetric monolayer of $Ti_3C_2T_x$ [31], with in-plane polarization p, because p and P are approximately perpendicular to each other and physically separated. In fact, p is in-plane and confined by the good electrical conductivity within the layers, while P is approximately perpendicular to and between the layers. In addition, while p is due to the atomic displacements within the layers, P is considered to arise from interlayer electronic transfer with minimal relative atomic displacements within layers [19].

In order to evaluate the effect of the transition on the elastic modulus, we include in the free energy the elastic and the mixed terms containing both P and strain ε or, considering the Gibbs free energy $G = F - \sigma\varepsilon$, the terms containing P and stress σ. Without entering in the details of the mechanism causing the polarization, we can safely include the electrostrictive coupling $Q\sigma P^2$, always allowed [37,52], while

the piezoelectric coupling $d\sigma p$ is with the intrinsic p, so that

$$G = \frac{a}{2}(T - T_C)P^2 + \frac{B}{4}P^4 + \frac{C}{6}P^6 + - \frac{S^0}{2}\sigma^2 - Q\sigma P^2 + \frac{1}{2\chi_p}p^2 - d\sigma p, \quad (2)$$

where the susceptibility χ_p of p, nearly independent of T, is included.

The elastic compliance $S = 1/E$ is calculated as usual [37,53,54] as $S = d\varepsilon/d\sigma$ with $\varepsilon = -\partial G/\partial\sigma$ and one obtains [36]

$$S(T > T_C) = S^0 + \chi_p d^2,$$
$$S(T < T_C) = S^0 + \chi_p d^2 + \Delta s,$$
$$\Delta S = \frac{2Q^2}{B\sqrt{\frac{T_C+\Delta T-T}{\Delta T}}}, \quad \Delta T = \frac{B^2}{4aC}. \quad (3)$$

The constant term $\chi_p d^2$ is the softening due to the intrinsic piezoelectricity, and just renormalizes the background compliance S^0. The coupling to P does not produce any effect in the paraelectric phase ($T > T_C$ for $B < 0$ and up to $T_C + \Delta T$ for $B < 0$), where P is null apart from fluctuations, and produces a steplike softening ΔS in the ferroelectric phase. The step is constant of magnitude $2Q^2/B$ if $C = 0$ and acquires a cusped shape for $C > 0$. This type of elastic anomaly is the same for any OP that is coupled quadratically to stress/strain, including magnetization and the rotation angle in antiferrodistortive transition, as in $SrTiO_3$ [40]. The softening is due to the relaxation of the order parameter upon application of stress, with consequent additional strain. In the FE case, the softening is of piezoelectric origin [54].

In view of the marked dependence on frequency shown in Fig. 3, the time dependence of the response of P to stress should be taken into account. This is usually done in the framework of the Landau-Khalatnikov theory, assuming that $\dot{P} = -(P - P_0)/(\chi L)$, where L is a nearly temperature-independent kinetic coefficient and χ the susceptibility $\sim|T - T_C|^{-1}$, yielding a relaxation time $\tau = \tau_0/(T_C - T)$. Introducing this time dependence of P into the elastic response to a periodic excitation with angular frequency ω yields a complex compliance $\Delta S/(1 + i\omega\tau)$ [40,55] and therefore a frequency dependence of the real part

$$\Delta S(\omega) = \Delta S/[1 + (\omega\tau)^2],$$
$$\tau = \tau_0/(T_C - T). \quad (4)$$

In order to fit the anomaly of the Young's modulus E with an expression like Eqs. (3)–(4), it is necessary to establish the background variation of $E(T)$. This usually is a linear stiffening during cooling, due to anharmonic effects, with quantum saturation below some temperature Θ, and can be written in terms of the compliance as [56]

$$1/E^0 = S^0 = S_0 + S_1/\tanh(\Theta/T). \quad (5)$$

However, additional phenomena affect $E(T)$, as apparent in Figs. 1 and 2, and therefore a fit cannot be extended above 500 K, where a smooth frequency-dependent kink is evident in Fig. 1. The low frequency experiment, spanning two decades in f, actually shows dependence of the background E^0 down to room temperature and is also noisier than in the resonance experiments. For this reason, we present a fit of the elastic anomaly measured during the third cooling run in resonance, when the sample had not yet been subjected to the various treatments with water. The best fit with Eqs. (3)–(5) is found with the parameters indicated in the caption to Fig. 4 (blue line). The red line is calculated at 1 Hz, in order to show the effect of the relaxation of the order parameter: increasing frequency, the minimum shifts to temperatures lower than T_C, and its magnitude decreases. This is of the same type as observed in Fig. 3, though its full magnitude cannot be reproduced with Eq. (4). It is possible that a contribution to softening below the transition is also given by the motion of domain walls, which is typically larger at lower frequency [40], and may well explain the larger magnitude of the step at lower frequency.

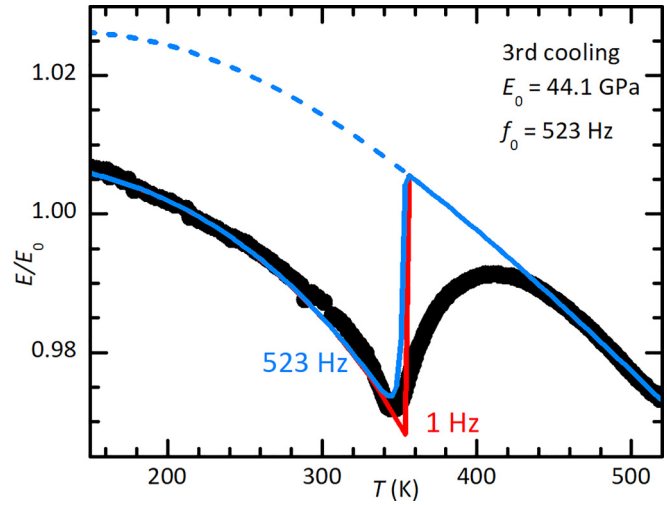

FIG. 4. Fit of the elastic anomaly presented in Fig. 1, measured at 523 Hz during the 3rd cooling, using Eq. (3) with the parameters $\Theta = 490$ K; $T_C = 354$ K, $\Delta T = 70$ K; $\Delta s \times E_0 = 0.039$, $\tau_0 = 7 \times 10^{-4}$ s. The red line is calculated at 1 Hz, The dashed line is the background E^0.

As anticipated, Eq. (3) does not contain the contribution of fluctuations above T_C, and therefore cannot reproduce the evident precursor softening. Precursor softening is found commonly, and in the classical ferroelectric $BaTiO_3$ it extends even to hundreds of kelvin above T_C [49]. It is notable that the Curie temperatures reported up to now for sliding ferroelectrics, WSe_2 [51] and WTe_2 [13,17], are $T_C \simeq 350$ K as in our case.

These measurements demonstrate that nanoscale phenomena like FE in mono- and bilayers of vdW solids, generally studied with advanced techniques at the nanoscale, can be probed with mechanical spectroscopy on thick films. Notice that it is not necessary that the direction of the interlayer polarization is coherent along different pairs of layers, since strain is coupled to P^2 and strains from opposite polarizations do not cancel with each other.

The dissipation $Q^{-1}(T)$ of $Ti_3C_2T_x$ presents a positive step below T_C, which is the normal behavior from the interaction between stress and the walls between the domains formed in the low-temperature phase [38,40,47]. With increase of

temperature, the dissipation is dominated by intense relaxation processes with a broad spectrum of characteristic times toward high temperature (P2 in Fig. 1). Among the possible contributions to these losses are relative sliding of the flakes, hopping of the residual intercalated species, diffusion of the terminating molecules, and motion of point and extended defects within the monolayers.

The magnitude of the Young's modulus of the film consolidated in high vacuum at 970 K, $E = 40-50$ GPa, is larger than that achieved in $Ti_3C_2T_x$, densified by addition of sodium carboxymethyl cellulose and sodium borate (28 GPa) [57] or carboxymethylated cellulose nanofibrils (42 GPa) [58], but the films are fragile and E is still one order of magnitude smaller than the 330 GPa found with AFM on single flakes [59]. The large discrepancy between the in-plane Young's modulus of single and aggregated flakes must be due to their easy relative sliding.

V. CONCLUSIONS

We measured for the first time the temperature dependence of the complex Young's modulus E of the $Ti_3C_2T_x$ MXene in the form of self-standing thick films. In the as-prepared state the films have a very low $E \sim 4-10$ GPa, that may be increased up to $40-50$ GPa by annealing in high vacuum at 970 K, so reducing the amount of intercalated species. This is still lower than 330 GPa of a single flake, presumably due to an easy relative sliding of the flakes, but allows reproducible anelastic spectra to be measured up to 900 K. The major feature is a phase transition below $T_C \sim 350$ K, producing a steplike softening of $\sim$4% of E and increase of dissipation, which is robust against thermal treatments up to 900 K in vacuum or inert gas. The nature of the phase transition is discussed and it is concluded that it should be ferroelectric, based on the fact that the available structural and magnetic measurements exclude deviations from the hexagonal structure and magnetism at room temperature. Particular attention has been devoted to the mechanism of sliding ferroelectricity, where sliding of the layers with respect to each other induces charge transfer between atoms/molecules belonging to the facing layers and hence to interlayer polarization. Notably, $T_C \simeq 350$ K is the same of two other known sliding ferroelectrics, WSe_2 [51] and WTe_2 [13,17]. This would add a new feature and perspectives of applications to the already numerous ones of $Ti_3C_2T_x$ MXene. In this view, the simple fact that this transition is slightly above room temperature calls for further investigations of its nature.

ACKNOWLEDGMENT

F.C. and A.D.C. acknowledge the precious technical assistance of M. P. Latino (CNR-ISM).

[1] G. Dong, S. Li, M. Yao, Z. Zhou *et al.*, Super-elastic ferroelectric single-crystal membrane with continuous electric dipole rotation, Science **366**, 475 (2019).

[2] S. H. Park, J. Y. Kim, J. Y. Song, and H. W. Jang, Overcoming size effects in ferroelectric thin films, Adv. Phys. Res. **2**, 2200096 (2023).

[3] D. Ji, S. Cai, T. R. Paudel, H. Sun *et al.*, Freestanding crystalline oxide perovskites down to the monolayer limit, Nature (London) **570**, 87 (2019).

[4] R. Fei, W. Kang, and L. Yang, Ferroelectricity and phase transitions in monolayer group-IV monochalcogenides, Phys. Rev. Lett. **117**, 097601 (2016).

[5] A. Belianinov, Q. He, A. Dziaugys, P. Maksymovych *et al.*, $CuInP_2S_6$ room temperature layered ferroelectric, Nano Lett. **15**, 3808 (2015).

[6] F. Liu, L. You, K. L. Seyler, X. Li *et al.*, Room-temperature ferroelectricity in $CuInP_2S_6$ ultrathin flakes, Nat. Commun. **7**, 12357 (2016).

[7] S. Wan, Y. Li, W. Li, X. Mao, W. Zhu, and H. Zeng, Room-temperature ferroelectricity and a switchable diode effect in two-dimensional α-In_2Se_3 thin layers, Nanoscale **10**, 14885 (2018).

[8] F. Sui, M. Jin, Y. Zhang, R. Qi *et al.*, Sliding ferroelectricity in van der Waals layered γ-InSe semiconductor, Nat. Commun. **14**, 36 (2023).

[9] N. Higashitarumizu, H. Kawamoto, C.-J. Lee, B.-H. Lin *et al.*, Purely in-plane ferroelectricity in monolayer SnS at room temperature, Nat. Commun. **11**, 2428 (2020).

[10] K. Chang, J. Liu, H. Lin, N. Wang *et al.*, Discovery of robust in-plane ferroelectricity in atomic-thick SnTe, Science **353**, 274 (2016).

[11] S. Yuan, X. Luo, H. L. Chan, C. Xiao, Y. Dai, M. Xie, and J. Hao, Room-temperature ferroelectricity in $MoTe_2$ down to the atomic monolayer limit, Nat. Commun. **10**, 1775 (2019).

[12] A. Lipatov, P. Chaudhary, Z. Guan, H. Lu *et al.*, Direct observation of ferroelectricity in two-dimensional MoS_2, npj 2D Mater. Appl. **6**, 18 (2022).

[13] Z. Fei, W. Zhao, T. A. Palomaki, B. Sun *et al.*, Ferroelectric switching of a two-dimensional metal, Nature (London) **560**, 336 (2018).

[14] P. Sharma, F.-X. Xiang, D.-F. Shao, D. Zhang, E. Y. Tsymbal, A. R. Hamilton, and J. Seidel, A room-temperature ferroelectric semimetal, Sci. Adv. **5**, eaax5080 (2019).

[15] M. V. Stern, Y. Waschitz, W. Cao, I. Nevo *et al.*, Interfacial ferroelectricity by van der Waals sliding, Science **372**, 1462 (2021).

[16] A. Weston, E. G. Castanon, V. Enaldiev, F. Ferreira *et al.*, Interfacial ferroelectricity in marginally twisted 2D semiconductors, Nat. Nanotechnol. **17**, 390 (2022).

[17] Q. Yang, M. Wu, and J. Li, Origin of two-dimensional vertical ferroelectricity in WTe_2 bilayer and multilayer, J. Phys. Chem. Lett. **9**, 7160 (2018).

[18] M. Wu and J. Li, Sliding ferroelectricity in 2D van der Waals materials: Related physics and future opportunities, Proc. Natl. Acad. Sci. USA **118**, e2115703118 (2021).

[19] S. Li, F. Wang, Y. Wang, J. Yang *et al.*, Van der waals ferroelectrics: Theories, materials and device applications, Adv. Mater. 2301472 (2023).

[20] Z. Wang, Z. Gui, and L. Huang, Sliding ferroelectricity in bilayer honeycomb structures: A first-principles study, Phys. Rev. B **107**, 035426 (2023).

[21] L. Yang, S. Ding, J. Gao, and M. Wu, Atypical sliding and moiré ferroelectricity in pure multilayer graphene, Phys. Rev. Lett. **131**, 096801 (2023).

[22] L. Li and M. Wu, Binary compound bilayer and multilayer with vertical polarizations: Two-dimensional ferroelectrics, multiferroics, and nanogenerators, ACS Nano **11**, 6382 (2017).

[23] J. Parker and Y. Gu, Van der Waals ferroelectrics: Progress and an outlook for future research directions, J. Appl. Phys. **132**, 160901 (2022).

[24] P. Tang and G. E. W. Bauer, Sliding phase transition in ferroelectric van der Waals bilayers, Phys. Rev. Lett. **130**, 176801 (2023).

[25] A. Bhat, S. Anwer, K. S. Bhat, M. I. H. Mohideen, K. Liao, and A. Qurashi, Prospects challenges and stability of 2D MXenes for clean energy conversion and storage applications, npj 2D Mater. Appl. **5**, 61 (2021).

[26] G. Li, S. Lian, J. Wang, G. Xie, N. Zhang, and X. Xie, Surface chemistry engineering and the applications of MXenes, J. Materiomics **9**, 1160 (2023).

[27] A. Agresti, A. Pazniak, S. Pescetelli, A. D. Vito *et al.*, Titanium-carbide MXenes for work function and interface engineering in perovskite solar cells, Nat. Mater. **18**, 1228 (2019).

[28] K. Hantanasirisakul and Y. Gogotsi, Electronic and optical properties of 2D transition metal carbides and nitrides (MXenes), Adv. Mater. **30**, 1804779 (2018).

[29] Y. Wang, T. Guo, Z. Tian, L. Shi, S. C. Barman, and H. N. Alshareef, MXenes for soft robotics, Matter **6**, 2807 (2023).

[30] A. Chandrasekaran, A. Mishra, and A. K. Singh, Ferroelectricity, antiferroelectricity, and ultrathin 2D electron/hole gas in multifunctional monolayer MXene, Nano Lett. **17**, 3290 (2017).

[31] D. Tan, C. Jiang, N. Sun, J. Huang *et al.*, Piezoelectricity in monolayer MXene for nanogenerators and piezotronics, Nano Energy **90**, 106528 (2021).

[32] D. Tan, N. Sun, L. Chen, J. Bu, and C. Jiang, Piezoelectricity in monolayer and multilayer $Ti_3C_2T_x$ MXenes: Implications for piezoelectric devices, ACS Appl. Nano Mater. **5**, 1034 (2022).

[33] A. Lipatov, M. Alhabeb, M. R. Lukatskaya, A. Boson, Y. Gogotsi, and A. Sinitskii, Effect of synthesis on quality, electronic properties and environmental stability of individual monolayer Ti_3C_2 MXene flakes, Adv. Electron. Mater. **2**, 1600255 (2016).

[34] F. Cordero, L. Dalla Bella, F. Corvasce, P. M. Latino, and A. Morbidini, An insert for anelastic spectroscopy measurements from 80 K to 1100 K, Meas. Sci. Technol. **20**, 015702 (2009).

[35] A. S. Nowick and B. S. Berry, *Anelastic Relaxation in Crystalline Solids* (Academic Press, New York, 1972).

[36] See Supplemental Material at http://link.aps.org/supplemental/10.1103/PhysRevB.109.024105 for details on: anelastic measurements with free flexural resonance; preliminary anelastic measurements and flattening anneal; the effect of water vapor and immersion in water on the anelastic spectra; XRD, RAMAN, SEM; calculation of the elastic anomaly in the Landau theory. It also contains Refs. [59,60].

[37] W. Rehwald, The study of structural phase transitions by means of ultrasonic experiments, Adv. Phys. **22**, 721 (1973).

[38] M. A. Carpenter and E. H. K. Salje, Elastic anomalies in minerals due to structural phase transitions, Eur. J. Mineral. **10**, 693 (1998).

[39] W. Schranz, H. Kabelka, and A. Tröster, Superelastic softening of ferroelastic multidomain crystals, Ferroelectrics **426**, 242 (2012).

[40] A. V. Kityk, W. Schranz, P. Sondergeld, D. Havlik, E. K. H. Salje, and J. F. Scott, Low-frequency superelasticity and nonlinear elastic behavior of $SrTiO_3$ crystals, Phys. Rev. B **61**, 946 (2000).

[41] H. Jin, K. Wang, Z. Mao, L. Tang, J. Zhang, and X. Chen, The structural, magnetic, Raman and electrical transport properties of Mn intercalated $Ti_3C_2T_x$, J. Phys.: Condens. Matter **34**, 015701 (2022).

[42] D. Sen, G. Jana, N. Kaushal, A. Mukherjee, and T. Saha-Dasgupta, Intrinsic ferromagnetism in atomically thin two-dimensional organic-inorganic van der Waals crystals, Phys. Rev. B **102**, 054411 (2020).

[43] J. A. McNulty and P. Lightfoot, Structural chemistry of layered lead halide perovskites containing single octahedral layers, IUCrJ **8**, 485 (2021).

[44] A. M. Glazer, The classification of tilted octahedra in perovskites, Acta Cryst. B **28**, 3384 (1972).

[45] T. Hu, Z. Li, M. Hu, J. Wang, Q. Hu, Q. Li, and X. Wang, Chemical origin of termination-functionalized MXenes: $Ti_3C_2T_2$ as a case study, J. Phys. Chem. C **121**, 19254 (2017).

[46] C. Shi, M. Beidaghi, M. Naguib, O. Mashtalir, Y. Gogotsi, and S. J. L. Billinge, Structure of nanocrystalline Ti_3C_2 MXene using atomic pair distribution function, Phys. Rev. Lett. **112**, 125501 (2014).

[47] F. Cordero, Quantitative evaluation of the piezoelectric response of unpoled ferroelectric ceramics from elastic and dielectric measurements: Tetragonal $BaTiO_3$, J. Appl. Phys. **123**, 094103 (2018).

[48] F. Cordero, F. Trequattrini, F. Craciun, H. T. Langhammer, D. A. B. Quiroga, and P. S. Silva Jr., Probing ferroelectricity in highly conducting materials through their elastic response: Persistence of ferroelectricity in metallic $BaTiO_{3-\delta}$, Phys. Rev. B **99**, 064106 (2019).

[49] F. Cordero, F. Trequattrini, P. S. da Silva Jr., M. Venet, O. Aktas, and E. K. H. Salje, Elastic precursor effects during $Ba_{1-x}Sr_xTiO_3$ ferroelastic phase transitions, Phys. Rev. Res. **5**, 013121 (2023).

[50] J. Xiao, H. Zhu, Y. Wang, W. Feng *et al.*, Intrinsic two-dimensional ferroelectricity with dipole locking, Phys. Rev. Lett. **120**, 227601 (2018).

[51] Y. Liu, S. Liu, B. Li, W. J. Yoo, and J. Hone, Identifying the transition order in an artificial ferroelectric van der Waals heterostructure, Nano Lett. **22**, 1265 (2022).

[52] M. E. Lines and A. M. Glass, *Principles and Applications of Ferroelectrics and Related Materials* (Oxford University Press, Oxford, UK, 1977).

[53] B. A. Strukov and A. P. Levanyuk, *Ferroelectric Phenomena in Crystals* (Springer, Heidelberg, 1998).

[54] F. Cordero, F. Craciun, F. Trequattrini, and C. Galassi, Piezoelectric softening in ferroelectrics: Ferroelectric versus antiferroelectric $PbZr_{1-x}Ti_xO_3$, Phys. Rev. B **93**, 174111 (2016).

[55] R. M. Yevych, Y. M. Vysochanskii, M. M. Khoma, and S. I. Perechinskii, Lattice instability at phase transitions near the Lifshitz point in proper monoclinic ferroelectrics, J. Phys.: Condens. Matter **18**, 4047 (2006).

[56] E. Salje, B. Wruck, and H. Thomas, Order-parameter saturation and low-temperature extension of Landau theory, Z. Phys. B **82**, 399 (1991).

[57] S. Wan, X. Li, Y. Chen, N. Liu *et al.*, High-strength scalable MXene films through bridging-induced densification, Science **374**, 96 (2021).

[58] W. Tian, A. V. Mohammadi, M. S. Reid, Z. Wang *et al.*, Multifunctional nanocomposites with high strength and capacitance using 2D MXene and 1D nanocellulose, Adv. Mater. **31**, 1902877 (2019).

[59] A. Lipatov, H. Lu, M. Alhabeb, B. Anasori, A. Gruverman, Y. Gogotsi, and A. Sinitskii, Elastic properties of 2D $Ti_3C_2T_x$ MXene monolayers and bilayers, Sci. Adv. **4**, eaat0491 (2018).

[60] N. C. Osti, M. Naguib, A. Ostadhossein, Y. Xie *et al.*, Effect of metal ion intercalation on the structure of MXene and water dynamics on its internal surfaces, ACS Appl. Mater. Interfaces **8**, 8859 (2016).